J Nanopart Res (2009) 11:1441–1452
DOI 10.1007/s11051-008-9531-8

RESEARCH PAPER

Fabrication and characterization of iron oxide nanoparticles filled polypyrrole nanocomposites

Zhanhu Guo · Koo Shin · Amar B. Karki · David P. Young · Richard B. Kaner · H. Thomas Hahn

Received: 8 July 2008 / Accepted: 2 October 2008 / Published online: 31 October 2008

Abstract The effect of iron oxide nanoparticle addition on the physicochemical properties of the polypyrrole (PPy) was investigated. In the presence of iron oxide nanoparticles, PPy was observed in the form of discrete nanoparticles, not the usual network structure. PPy showed crystalline structure in the nanocomposites and pure PPy formed without iron oxide nanoparticles. PPy exhibited amorphous structure and nanoparticles were completely etched away in the nanocomposites formed with mechanical stirring over a 7-h reaction. The thermal stability of the PPy in the nanocomposites was enhanced under the thermo-gravimetric analysis (TGA). The electrical conductivity of the nanocomposites increased greatly upon the initial addition (20 wt%) of iron oxide nanoparticles. However, a higher nanoparticle loading (50 wt%) decreased the conductivity as a result of the dominance of the insulating iron oxide nanoparticles. Standard four-probe measurements indicated a three-dimensional variable-range-hopping conductivity mechanism. The magnetic properties of the fabricated nanocomposites were dependent on the particle loading. Ultrasonic stirring was observed to have a favorable effect on the protection of iron oxide nanoparticles from dissolution in acid. A tight polymer structure surrounds the magnetic nanoparticles, as compared to a complete loss of the magnetic iron oxide nanoparticles during conventional mechanical stirring for the micron-sized iron oxide particles filled PPy composite fabrication.

Keywords Polymer nanocomposites · Conductivity · Stirring methods · Magnetic property · Thermal stability · Corrosion-resistance · Nanomanufacturing

Z. Guo · H. T. Hahn
Multifunctional Composites Lab (MCL), Mechanical & Aerospace Engineering and Materials Science & Engineering Department, University of California, Los Angeles, CA 90095, USA

Present Address:
Z. Guo (✉)
Chemical Engineering Department, Lamar University, Beaumont, TX 77710, USA
e-mail: zhanhu.guo@lamar.edu

K. Shin
Department of Applied Chemistry, Sejong University, Seoul 143-747, South Korea

A. B. Karki · D. P. Young
Department of Physics and Astronomy, Louisiana State University, Baton Rouge, LA 70803, USA

R. B. Kaner
Department of Chemistry and Biochemistry, University of California, Los Angeles, CA 90095, USA

Introduction

Polypyrrole (PPy), a conducting conjugated polymer, has attracted much interest due to its low cost, easy synthesis, good stability, and environmentally benign

performance (Yeh et al. 2003). The conductivity of a conductive polymer is strongly dependent on the doping agents (dopant) with electron donor or acceptor abilities. The doping process can even transform an intrinsically conjugated polymer insulator to a near-metallic conductor (Lee et al. 2006). Conductive PPy has been reported to serve as polymeric rechargeable batteries for energy-storage purposes (Song and Palmore 2006), electrode materials used in the electrochemical supercapacitors (Ingram et al. 2004; Noh et al. 2003), metal corrosion protection coating materials (Ferreira et al. 1990; Zaid et al. 1994), matrix for structural composite materials (Han et al. 2005), electromagnetic interference (EMI) shielding, electrochemomechanical devices (Asavapiriyanont et al. 1984), and sensors for pH (Lakard et al. 2007), gas, and humidity (Tandon et al. 2006; An et al. 2004) testing. In addition, granular polypyrrole nanocomposites have been reported as a candidate for photovoltaic (solar cell) materials (Kwon et al. 2004).

Polymer nanocomposites with nanoparticles (NPs) have attracted much interest due to their homogeneity, easy processability, and tunable physical (mechanical, magnetic, electrical, thermoelectric, and electronic) properties (Castro et al. 2000; Wang et al. 2000; Gangopadhyay et al. 2000; Corbierre et al. 2001; Li et al. 2002; Wetzel et al. 2003; Mack et al. 2005; Chen et al. 2005; Vivekchand et al. 2005; Mammeri et al. 2005; Guo et al. 2006; Lee et al. 2008). High particle loading is required for certain industrial applications, such as electromagnetic wave absorbers (Brosseau and Talbot 2005; Guo et al. 2007a), photovoltaic cells (solar cells) (Beek et al. 2004), photo detectors, and smart structures (Gall et al. 2004; Mohr et al. 2006; Guo et al. 2007b). Magnetic nanoparticles, due to their unique magnetic and electronic properties, are used in various applications such as biomedical drug delivery, specific site targeting, magnetic data storage and sensors (Toal and Trogler 2006; Podlaha et al. 2006; Lei and Bi. 2007; Bi et al. 2008). Successfully incorporating magnetic nanoparticles into conductive polymer matrices will definitely widen their applicability in the fields of electronics, biomedical drug delivery, and optics. However, one of the challenges so far is the ability to integrate a high fraction of nanoparticles into the polymer matrix in a strong acidic environment. The acid, which is normally required for the PPy synthesis, will etch away the nanoparticles in aqueous solutions. A balance between the need for polymerization in an acidic solution and the prevention of dissolution of reactive iron oxide nanoparticles will be a determining factor for high-quality nanocomposite fabrication.

Polypyrrole nanocomposites with iron oxide and other nanoparticles have been prepared by several methods. For example, an in situ chemical oxidative polymerization approach with either an ultrasonication approach (Yen et al. 2008) or mechanical stirring approach (Li et al. 2006) was reported. The nanocomposites showed particle-loading magnetic properties and electric conductivity. In addition, the supercritical fluid was also reported to be used as a media in the in situ chemical oxidative polymerization for the fabrication of the conductive polymer magnetic nanocomposites with a consideration of green chemistry (Yuvaraj et al. 2008). The stirring method (ultrasonication or mechanical stirring) is believed to have a significant effect on the formed nanocomposites and the subsequent physicochemical properties. However, there are few papers reported in the literature.

In this paper, the effect of iron oxide nanoparticle addition on the morphology of PPy, thermal stability, magnetic properties, and electrical conductivity of the resulting Fe_2O_3/PPy nanocomposites was reported. The effect of the stirring method, i.e., ultrasonic and mechanical stirring on the composite fabrication was also reported. The electric conductivity was investigated by a standard four-probe method and found to be strongly dependent on the particle loadings. The iron oxide nanoparticles were observed to be stable even after exposure to a strong acid with a pH value of 1.0 for more than 3 weeks.

Experimental details

Materials

The pyrrole monomer (Aldrich) was distilled under reduced pressure. γ-Fe_2O_3 nanoparticles were obtained from Nanophase Technologies Corporation with a reported average size of 23 nm and a specific surface area of 45 m^2/g. Ammonium persulfate (APS) and *p*-toluenesulfonic acid ($CH_3C_6H_4SO_3H$, *p*-TSA) were all purchased from Aldrich and used as received without further treatment.

Polypyrrole and nanocomposite preparation

A dispersion of γ-Fe_2O_3 nanoparticles was made by adding a desired amount of γ-Fe_2O_3 in 20 mL deionized water under sonication. The *p*-TSA (6.0 mmol) and pyrrole (7.3 mmol) were added into the above nanoparticle suspended solution under constant sonication and continuously stirred for 10 min. APS (3.6 mmol) was rapidly mixed into the above solution at room temperature, and the resulting solution was kept under sonication for 1 h. In addition, the effect of reaction time was investigated by sonication for 7 h as used previously in a study of the micron-sized iron oxide particles (Li et al. 2006). Both mechanical and ultrasonic stirring were explored, and the resulting nanocomposite properties were characterized accordingly. All the products were washed thoroughly with deionized water (to remove any unreacted APS and *p*-TSA) and methanol (to remove any oligomers), respectively. The precipitated powder was dried at 50 °C for further analysis. As a control experimental for comparison purposes, pure PPy was also synthesized following the same procedure as described before but without iron oxide nanoparticles.

Characterization

A Fourier transform infrared (FT–IR) spectrometer (Jasco, FT–IR 420) in transmission mode under dry nitrogen flow (10 cubic centimeters per minute, ccpm) was used to test the physicochemical interactions between PPy and Fe_2O_3 nanoparticles. The dried PPy powder was mixed with powder KBr, ground, and compressed into a pellet. Its spectrum was recorded as a reference to be compared with that of the Fe_2O_3/PPy nanocomposites.

The thermal degradation of the nanocomposites with different particle loadings was studied with a thermo-gravimetric analysis (TGA, Perkin Elmer). TGA was conducted on pure PPy and Fe_2O_3/PPy nanocomposites from 25 °C to 600 °C with an argon flow rate of 50 ccpm and a heating rate of 10 °C/min.

The dispersion quality of the nanoparticles within the PPy matrix, and the nanostructures of the polymer and nanocomposites were investigated using a scanning electron microscope (SEM, JEOL field emission scanning electron microscope, JSM-6700F). The SEM specimens were prepared by spreading a thin layer of powder onto a double-side carbon tape. The microstructure and crystallinity were investigated with a transmission electron microscope (TEM, JEOL, 100CX) with an accelerating voltage of 100 keV. The samples were prepared by dispersing the powder in anhydrous ethanol, dropping some suspended solution onto a carbon-coated copper grid and drying naturally under ambient conditions.

The magnetic properties of the nanocomposite were investigated in a 9-Tesla physical properties measurement system (PPMS) by Quantum Design. The electrical conductivities were measured using a standard four-probe method. The samples were prepared by the cold-press method. The applied pressure was 10,000 psi and the pressing duration time was 10 min.

Results and discussion

Figure 1 shows the SEM microstructures of the synthesized pure PPy and Fe_2O_3/PPy nanocomposites fabricated by the conventional method, as used for iron oxide micron-sized particles filled PPy composite fabrication (Li et al. 2006). The conventional method is based on mechanical stirring over a long period of time. In contrast to the network structure of pure PPy as shown in Fig. 1a, discrete spherical nanoparticles with uniform size distribution are observed in the nanocomposite counterparts fabricated by the conventional method as shown in Fig. 1b. However, no attraction was observed when a permanent magnet was placed nearby, and further quantitative magnetic characterization did not show any sign of magnetization in the nanocomposite. The disappearance of the magnetic iron oxide nanoparticles is believed to be due to the slow dissolution over time caused by the acidic solution used in the pyrrole polymerization. This observation also suggests the formation of a porous PPy shell rather than a solid tight one that can protect the magnetic nanoparticles from dissolution.

For the in situ formation of the conductive magnetic nanocomposite, a short reaction time (1 h) was used to balance the PPy formation and the iron oxide nanoparticle dissolution. Ultrasonic stirring was used rather than mechanical stirring to minimize the contamination and achieve better particle dispersion. The red particles turned black after the

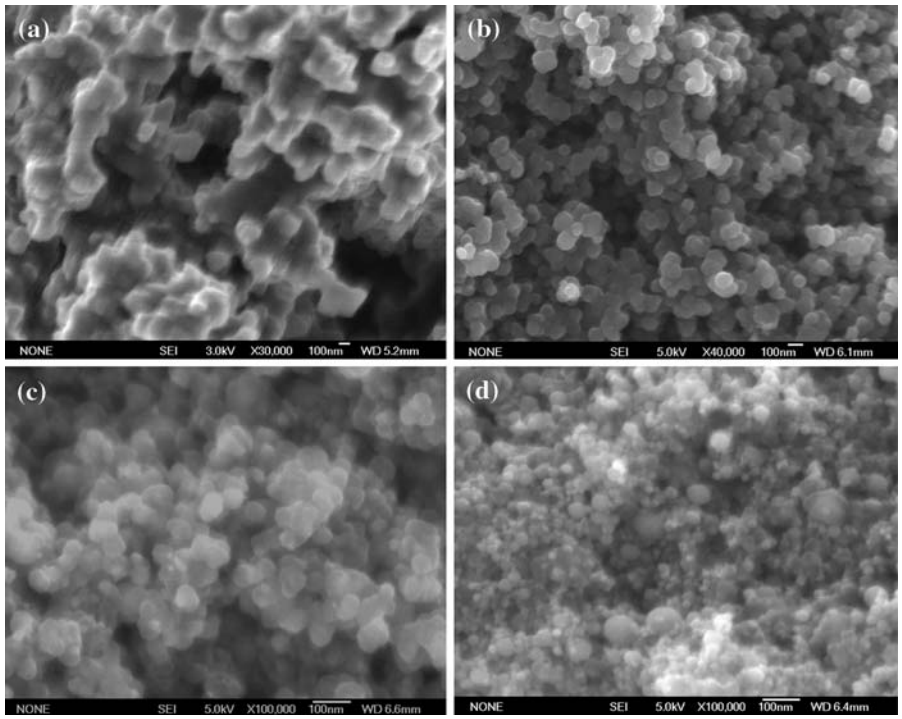

Fig. 1 SEM micrographs of **a** pure PPy formed without iron oxide nanoparticles, **b** pure PPy formed with iron oxide nanoparticles completely dissolved (mechanical stirring), **c** Fe_2O_3/PPy nanocomposites with 20 wt% iron oxide nanoparticles (sonication), and **d** Fe_2O_3/PPy nanocomposites with 50 wt% iron oxide nanoparticles (sonication)

polymerization, indicating the formation of PPy. Unlike the network structure as observed with pure PPy, the SEM micrographs as shown in Fig. 1c, d of the nanocomposites with different initial particle loadings show discrete nanoparticles without any obvious adhesion between them. In stark contrast to the obvious loss of magnetic nanoparticles when mechanical stirring was used for the 7-h polymerization, the dried nanocomposite powder in Fig. 1c, d did get attracted toward a permanent magnet, indicating the presence of the magnetic nanoparticles.

Figure 2 shows the FT–IR spectra of the pure PPy and Fe_2O_3/PPy nanocomposites. Characteristic peaks of PPy are observed in all the samples, indicating the formation of PPy. The peaks at 1547 and 1464 cm^{-1} can be assigned to C = C and C–N stretching vibrations, respectively. The peaks at 1,172 and 901 cm^{-1} are due to the C–H in-plane bending and ring deformation, respectively. Similar patterns were also observed in PPy-Fe[OH] microcomposites (Li et al. 2006). The obvious spectral differences between pure PPy and the composites indicate that PPy exhibits a different PPy chain structure and there are

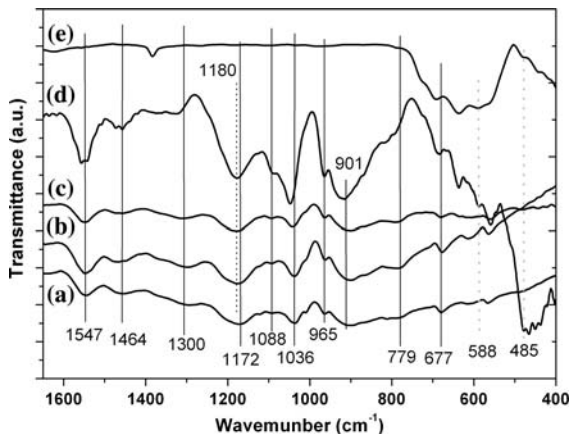

Fig. 2 FT–IR spectra of **a** pure PPy without nanoparticles, **b** PPy with iron oxide nanoparticles that have been attacked by acid, **c** a Fe_2O_3/PPy composite with a 20 wt% particle loading, **d** composite with a 50 wt% loading, and **e** as-received iron oxide nanoparticles

physicochemical interactions between the nanoparticles and PPy. The presence of iron oxide nanoparticles in the 20 and 50 wt% composites is strongly supported by new peaks at 485 cm^{-1} and 588 cm^{-1} as shown in

Fig. 2c, d, which are characteristic peaks of Fe_2O_3 (e.g., polyhedral Fe^{3+}–O^{2-} stretching vibrations of iron oxide) (Ram 1995; Sepulveda-guzman et al. 2007; Guo et al. 2007c). This observation indicates that a magnetic nanocomposite can be synthesized with PPy if polymerization can be achieved in a short period of time. The prolonged polymerization is characterized by the disappearance of the characteristic IR peaks of iron oxide as shown in Fig. 2b. The almost similar spectra between the PPy and PPy fabricated by the long time reaction also indicate the loss of iron oxide nanoparticles.

The thermal stability of pure PPy and Fe_2O_3/PPy nanocomposites was investigated by TGA measurements. Figure 3a shows the thermogravimetric profiles of nanocomposites with different particle loadings (0, 20, and 50 wt%). The black nanocomposites were observed to turn red upon test completion, characteristic of iron oxide rather than black carbon, indicating the complete loss of PPy. The weight loss at temperatures lower than 120 °C is due to loss of moisture, while the major loss at temperatures higher than 240 °C is due to the decomposition of PPy. The differences in the residue reflect the different amounts of iron oxide nanoparticles present. In addition, pure PPy formed with the aid of iron oxide nanoparticles shows higher stability than that formed without them. The thermal stability increases slightly with increasing nanoparticle loading, which is believed to be due to both the lower mobility of the polymer chains when the polymer chains are bound onto the nanoparticles and stronger chemical interaction (Chen et al. 2003). Similar to the TGA observation, a higher decomposition temperature (308.0 °C) as shown in Fig. 3b was observed in the PPy formed with the aid of nanoparticles than that (298.4 °C) of the pure PPy formed without them. Whereas only one peak was observed in the pure PPy samples, two exothermic peaks are observed in the DTA curves of the nanocomposites. These are due to the decomposition of PPy at 307 °C and the possible phase transition of iron oxide at 480 °C, as reported in the Fe_2O_3/PPy nanocomposites fabricated by the simultaneous gelation and polymerization (sol-gel) method (Suri et al. 2001; Suri et al. 2003), respectively. As compared with no obvious phase transition in the pure iron oxide nanoparticles, the observed phase transition is likely due to an intermediate product of PPy (Suri et al. 2001; Suri et al. 2003).

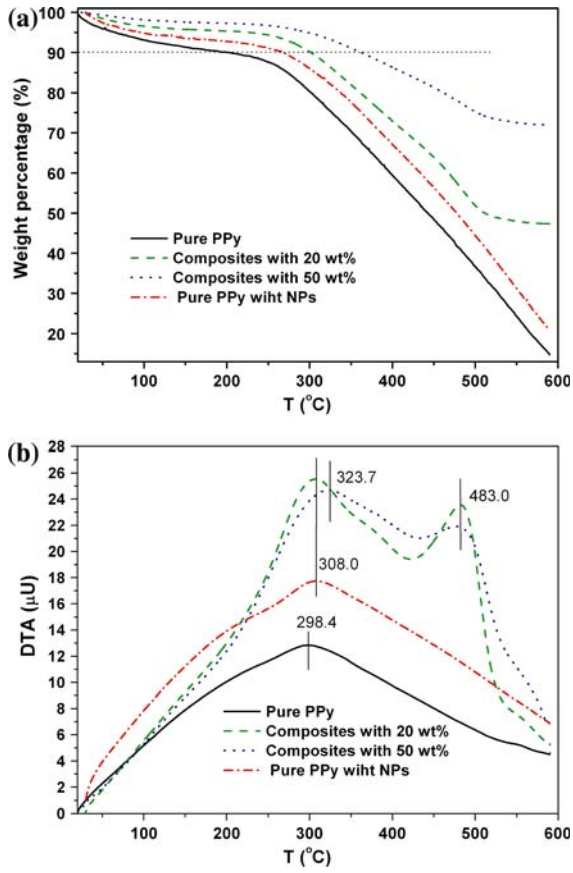

Fig. 3 **a** TGA weight changes and **b** corresponding DTA curves of pure PPy, and Fe_2O_3/PPy nanocomposites with different particle loadings

Figure 4 shows the magnetic hysteresis loops of the nanocomposites with an initial particle loading of 20 and 50 wt%, respectively. There is no hysteresis observed in the sample formed from the 7-h reaction due to the dissolution of magnetic nanoparticles in the acidic solution. The saturation magnetization (M_s) is about 29.4 emu/g and 45.1 emu/g based on the total weight of the nanocomposites with an initial loading of 20 and 50 wt%, respectively. The saturation magnetization of iron oxide was reported to be 74 emu/g and independent of the surface chemistry of the nanoparticles. Thus, the real particle loading of the nanoparticles in the nanocomposites with an initial particle loading of 20 and 50 wt% was calculated to be 27 and 68 wt%, respectively. The calculated particle loading based on the magnetic data is much higher than the initial particle loading considering the partial particle loss from the dissolution during the nanocomposite fabrication. This

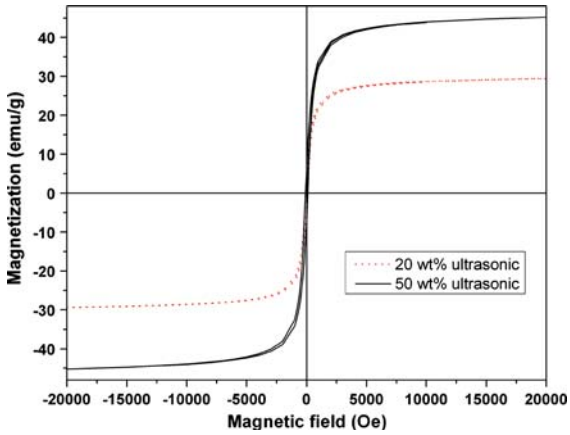

Fig. 4 Magnetic hysteresis loops of nanocomposites at different loadings

indicates that the yield of the PPy is lower. In other words, the pyrrole monomers are partially polymerized into PPy, which leads to higher particle loading. In addition, the polymer yield was observed to be lower at the higher initial particle loading than that at the lower initial particle loading.

The electrical conductivity was measured by a standard four-probe method. Figure 5a shows the temperature-dependent resistivity of pure PPy and nanocomposites with different particle loadings. The PPy synthesized with the presence of the nanoparticles over a long-term reaction was observed to have large resistance beyond the ability of the utilized equipment due to the poor contact between small particles (Dey et al. 2005) and the observed amorphous structure. At lower temperature the resistance is too large to be measured by the utilized equipment. The much lower resistivity in the pure PPy prepared by the conventional method is due to the network structure formation as shown in the SEM image of Fig. 1a, which favors electron transport. The resistivity change is not due to the doping extent based on the fact that all the samples were washed and doped with the same solution (Huang et al. 2005). The resistance was observed to decrease dramatically in the Fe_2O_3/PPy nanocomposites. The nanocomposite with an initial particle loading of 50 wt% was observed to have a higher resistivity, which is due to the known insulating properties of iron oxide (Ortiz et al. 1988; Mei et al. 1987) and consistent with the silicon carbide/polypyrrole nanocomposites (Omastova et al. 2005), silica/polypyrrole nanocomposites (Dutta and De 2006), and titanium dioxide/polyaniline nanocomposites (Su and Kuramoto 2000).

Figure 5b shows the temperature-dependent conductivity (σ). The conductivity of the pure PPy and nanocomposites with two different particle loadings can be linearly correlated to temperature with the quasi-three-dimensional variable range hopping (quasi-3D-VRH) model. The variable range hopping theory analysis indicates that three-dimensional hopping dominates in these samples, and the correlation between conductivity and temperature can be expressed in Eq. 1,

$$\sigma(T) = \sigma_0 \exp\left[-\left(\frac{T_0}{T}\right)^{1/4}\right] \quad (1)$$

where T_0 is the characteristic Mott temperature and the pre-exponential factor σ_0 is the conductivity at

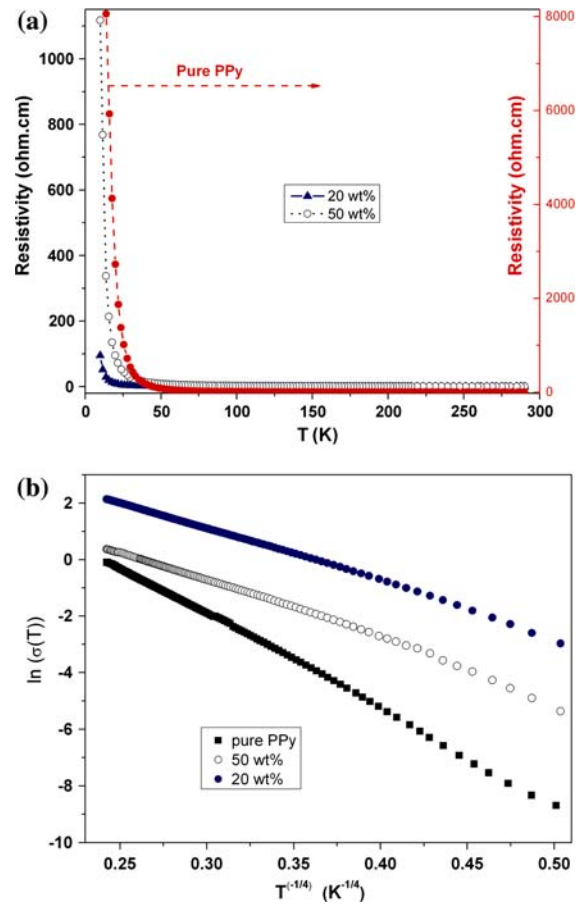

Fig. 5 Temperature-dependent **a** resistivity and **b** conductivity of pure PPy and nanocomposites with different loadings

infinite temperature. The σ_0 was calculated to be 3000.1 S cm^{-1}, 978.4 S cm^{-1}, and 298.8 S cm^{-1} for pure PPy and nanocomposites with an initial particle loading of 20 and 50 wt%, respectively. The T_0 was calculated to be 1204137, 138346, and 212010 K for pure PPy and the nanocomposites with an initial particle loading of 20 and 50 wt%, respectively. The parameter T_0 is inversely proportional to the localization length of the charge carriers. A larger T_0 implies a stronger localization of the charge carriers, which results in an increase of the resistance at low temperatures, whereas a small T_0 implies a weak localization (Gangopadhyay et al. 2000). The observed T_0 variation with the component is consistent with our observed resistivity changes in the synthesized PPy and Fe_2O_3/PPy systems.

It was reported that the electrical conductivity strongly depends on the ordered states of the conductive polymer (Abthagir and Saraswathi 2005). In other words, the structural and electronic properties of PPy can be easily modified due to a soft lattice, which can be reflected in the crystalline structure of the nanomaterials. Iron oxide nanoparticles are thought to serve as a template for the subsequent PPy matrix formation. Ultrasonic energy has been reported to have strong capability to alter the electronic structure of a polymer or even produce various nanoparticles. Here, the crystalline structural change with the nanocomposite formation was investigated using selected area electron diffraction (SAED) and dark field TEM microstructures. Figure 6a, b show the bright field TEM microstructure of pure PPy and the corresponding selected area electron diffraction (SAED). Similar to the SEM observation, linked nanoparticles were observed in the bright field TEM images as shown in Fig. 6a. The clear ring pattern as shown in Fig. 6b indicates a crystalline structure for the formed PPy. The lattice

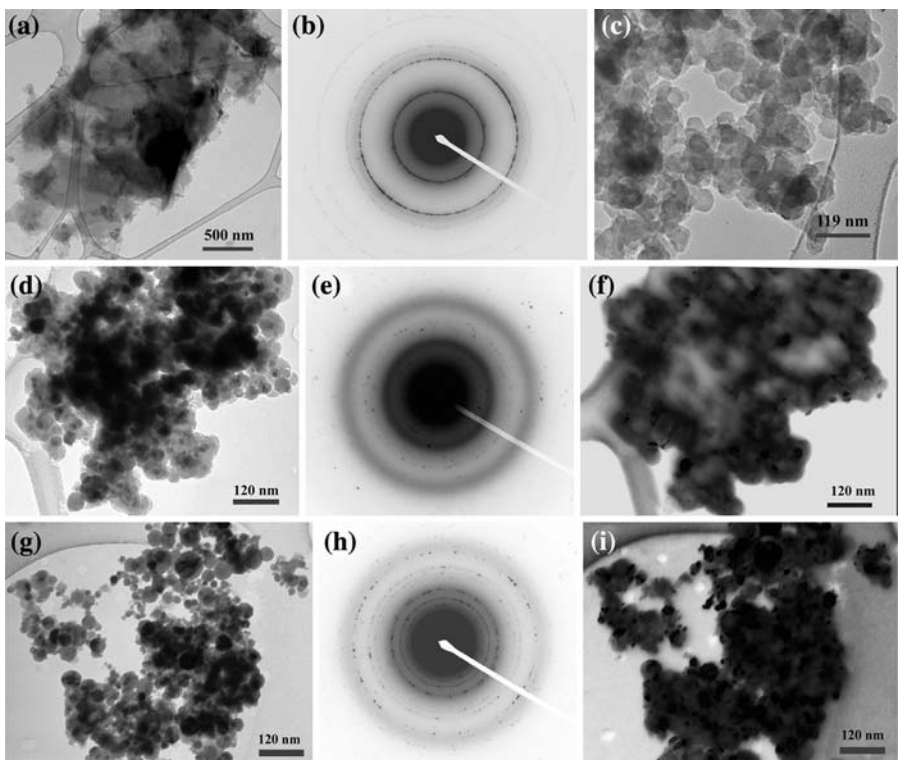

Fig. 6 **a** TEM bright field microstructure of pure PPy formed without iron oxide nanoparticles, **b** selected area electron diffraction (SAED) pattern of pure PPy in **a**, and **c** TEM bright field microstructure of PPy formed with iron oxide nanoparticles completely dissolved. **d** TEM bright field microstructure of the Fe_2O_3/PPy nanocomposites with an initial loading of 20 wt%, **e** SAED pattern of pure PPy in **d**, **f** dark field microstructure of the corresponding sample in **d**, **g** TEM bright field microstructure of the Fe_2O_3/PPy nanocomposites with an initial loading of 50 wt%, **h** SAED pattern of pure PPy in **g**, and **i** dark field microstructure of the corresponding sample in **g**

distances and crystalline planes (from the inner to the outward) of the pure PPy calculated from the electron diffraction patterns are 0.117 nm (100), 0.0666 nm (111), 0.0577 nm (200), 0.0434 nm (220), and 0.0386 nm (300), respectively. However, no ring pattern is observed in PPy formed in the presence of the iron oxide nanoparticles over a long time reaction, indicating an amorphous structure. The observed discrete spherical structure as shown in Fig. 7c is consistent with the SEM observation, which leads to poor contact and high resistivity.

Figure 6d–i shows the bright field microstructure, selected area electron diffraction, and dark field micrograph of the prepared nanocomposites with an initial particle loading of 20 and 50 wt%, respectively. Discrete nanoparticles are observed in the nanocomposites and consistent with the SEM observations. The image contrast arises from different molecular weights of PPy and iron oxide. The dark and gray regions correspond to iron oxide and PPy, respectively. The lattice distance of the related SAED of the nanocomposite with an initial particle loading of 20 wt% as shown in Fig. 6e is indexed to 0.167 nm (2 1 1, Fe_2O_3), 0.137 nm (2 0 8, Fe_2O_3), 0.114 nm (100. PPy), 0.086 nm (2 3 8, Fe_2O_3), and 0.0804 nm (2 4 4, Fe_2O_3). The SAED pattern of the nanocomposite with an initial particle loading of 50 wt% is indexed to 0. 167 nm (2 1 1, Fe_2O_3), 0.137 nm (2 0 8, Fe_2O_3), 0.111 nm (100, PPy), 0.0863 nm (2 3 8, Fe_2O_3), 0.0804 nm (2 4 4, Fe_2O_3), 0.0648 nm (111, PPy), 0.0569 nm (200, PPy), and 0.0376 nm (300, PPy). The dark field micrographs of the nanocomposites corresponding to the bright field images as shown in Fig. 6f, i also indicate a crystalline structure. The high crystallinity observed in the nanocomposites is most likely responsible for the increased conductivity. In addition, the lattice distance of PPy was observed to be smaller in the

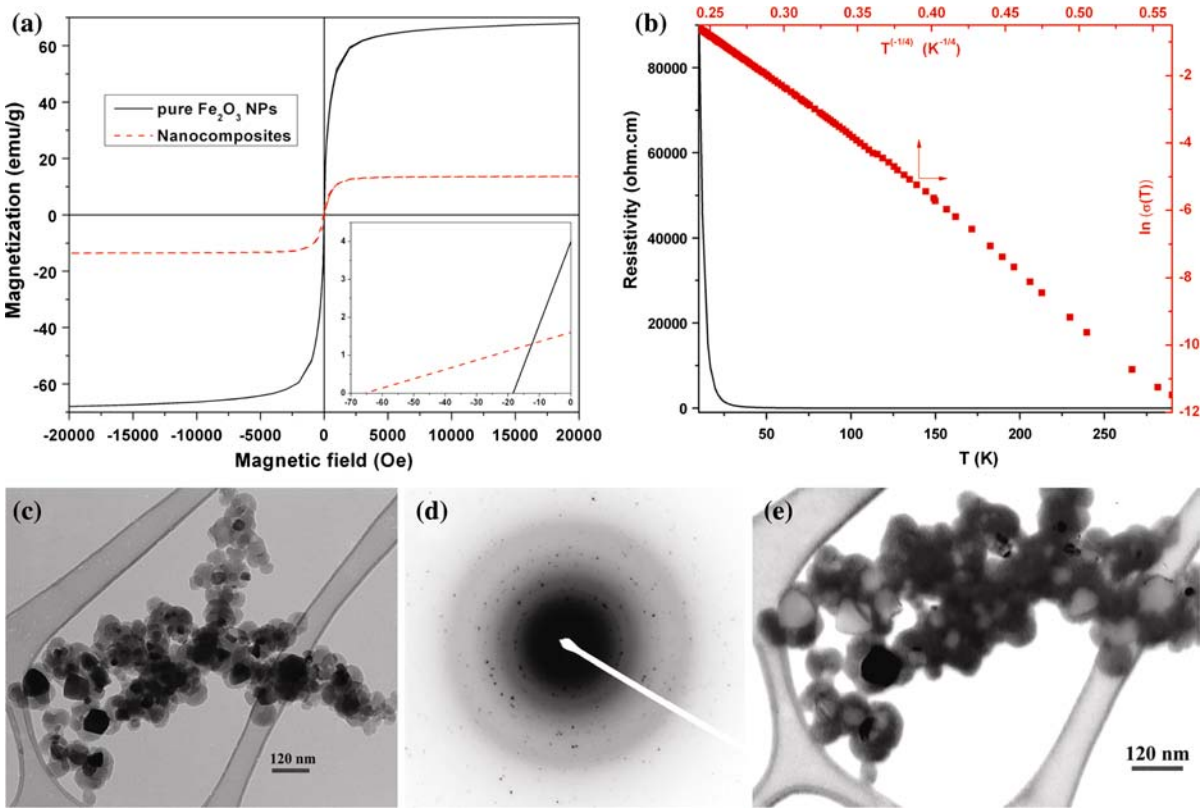

Fig. 7 **a** Magnetic hysteresis loops of pure iron oxide nanoparticles and the nanocomposite, **b** temperature-dependent resistivity/conductivity of the nanocomposite, **c** TEM bright field microstructure, **d** selected area electron diffraction (SAED) pattern, and **e** dark field microstructure of the Fe_2O_3/PPy nanocomposite (nanocomposite has an initial loading of 50 wt% and is ultrasonically stirred for 7 h)

nanocomposite with a higher particle loading, indicating that the nanoparticles favor a compact PPy structure with a lower resistivity. However, the high resistivity in the higher particle loaded nanocomposite is due to the insulating iron oxide nanoparticles, which dominate the electron transport at higher loadings.

The effect of the stirring method, i.e., mechanical versus ultrasonic stirring was investigated by polymerizing for 7 h as used in the mechanical stirring. The final product exhibits a strong attraction to a permanent magnet, indicating the presence of iron oxide nanoparticles. Figure 7a shows the hysteresis loop of the as-received iron oxide nanoparticles and the nanocomposite (an initial particle loading of 50 wt%) synthesized with ultrasonic stirring over 7 h, respectively. The weight percentage of iron oxide nanoparticles in the nanocomposite was estimated to be 20.2% based on the saturation magnetization of the nanocomposite and the as-received nanoparticles. This weight percentage is much lower than the initial particle loading and the composite sample synthesized with a 1-h ultrasonic stirring. This indicates that more particles are lost due to the dissolution over the long-time reaction between the nanoparticles and the protons. The coercivity was observed to be much larger in the nanocomposite (65 Oe) than in the as-received samples (18 Oe), due to the dispersion of the single-domain size nanoparticles. Figure 7b shows the temperature-dependent resistivity and conductivity (σ) of the nanocomposite with an initial particle loading of 50 wt% and ultrasonic stirring for 7 h. In comparison to the high resistivity of the nanoproduct (pure PPy, complete loss of the iron oxide nanoparticles), the lower resistivity and the presence of magnetic hysteresis indicate a significant effect of the stirring methods on the composite preparation, and the ultrasonic stirring favors the protection of nanoparticles from dissolution. The linear relation between ln(σ) and T^(−1/4) indicates a quasi-three-dimensional variable range hopping (quasi-3D-VRH) mechanism.

Figure 7c–e shows the bright field microstructures, corresponding selected area electron diffraction, and dark field microstructures of the nanocomposites with ultrasonic stirring, respectively. The contrast as shown in Fig. 7c represents iron oxide nanoparticles (black region) and polymer PPy (gray region). The nanoparticles are observed to be enclosed and protected from complete dissolution by the polymer matrix. The ring patterns with clear spots shown in Fig. 7d indicate the highly crystalline structure of the nanocomposites, which can be indexed to iron oxide nanoparticles and the formed PPy. The dark field microstructures of the nanocomposites also indicate a crystalline structure. The crystalline structural parameter of pure PPy and electric resistivity/conductivity of the nanocomposites are summarized in Table 1. The crystalline structural parameter is observed to be larger in the nanocomposites with a 7-h ultrasonic stirring and an initial particle loading of 50 wt%, which is due to the majority of the PPy matrix, as observed in the TEM (Fig. 7c) and also lower final iron oxide particle loading. With a similar crystalline structural parameter, the presence of iron oxide nanoparticles makes the nanomaterials less

Table 1 Physical properties of pure PPy and Fe_2O_3/PPy nanocomposites

Material name	Conductivity at 290 K (S cm^{-1})	Conductivity at 10 K (S cm^{-1})	Final particle loading (wt%)[d]
Pure PPy[a]	0.9	1.2×10^{-4}	0
Nanocomposite 20 wt%[b] (1 h ultrasonic stirring)	8.3	105.4×10^{-4}	27.0
Nanocomposite 50 wt% (1 h ultrasonic stirring)	1.4	9.0×10^{-4}	68.0
Nanocomposite 50 wt% (7 h ultrasonic stirring)	0.6	1.0×10^{-5}	20.2
Nanocomposite 50 wt%[c] (7 h mechanical stirring)	$<1.2 \times 10^{-10}$	$<1.2 \times 10^{-10}$	0

[a] Pure PPy formed without iron oxide nanoparticles

[b] The weight percentage was the initial particle loading before polymerization and calculated based on the total mass of monomers and the nanoparticles

[c] This is pure PPy and the nanoparticles were completely dissolved due to the reaction between the nanoparticles and the protons

[d] Particle loading was estimated from the saturation magnetization

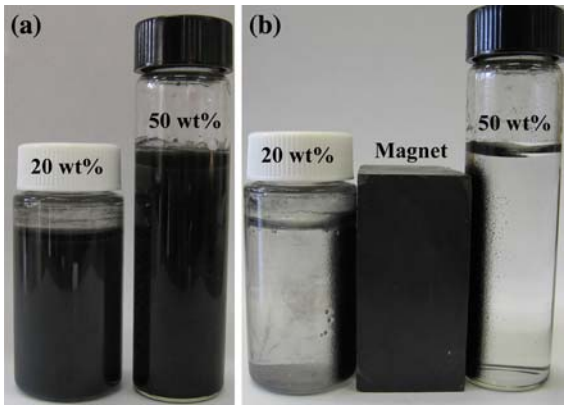

Fig. 8 **a** Nanocomposites redispersed in the aqueous solution, and **b** the attraction of the nanocomposite onto a permanent magnet in a hydrogen chloride solution

conductive. With an amorphous structure, PPy formes, with the presence of iron oxide nanoparticles and long-time mechanical stirring, insulating materials.

The stability of the Fe_2O_3/PPy nanocomposites in harsh environments was tested by dispersing the nanocomposites in an aqueous hydrogen chloride solution with a pH value of 1.0 for more than 3 weeks. The nanocomposites were observed to be re-dispersible in water as shown in Fig. 8a and exhibited a strong tendency to be attracted onto the permanent magnet as shown in Fig. 8b. This indicates that the iron oxide nanoparticles in the nanocomposites have been effectively protected by the formed PPy during the ultrasonic stirring polymer formation, in stark contrast with the complete loss of the nanoparticles in the mechanical stirring composite sample. In addition, the nanocomposites were attracted to the magnet very quickly, and the black solution turned to transparent within minutes. The stabilized iron oxide nanoparticles within the conductive polymer matrix in acidic environments allow these nanocomposites to be used in biomedical areas.

Summary

The effect of iron oxide nanoparticles on the chemical polymerization of pyrroles in an acidic solution was investigated and found to significantly influence the morphology (size and shape) and other physicochemical properties of the PPy. Pure discrete PPy nanoparticles with a much higher resistivity are formed over a long reaction time in the presence of iron oxide nanoparticles. Similar to pure PPy formed with iron oxide nanoparticles and different from the network structure of the pure PPy formed without iron oxide nanoparticles, discrete nanoparticles are observed in all the nanocomposites with an initial particle loading of 20 and 50 wt%. The subsequent nanocomposites are observed to have an improved thermal stability with a higher decomposition temperature. FT–IR, TGA/DTA, and TEM/SAED analyses indicate a strong interaction between the iron oxide nanoparticles and the polymer matrix. PPy was observed to have a lower yield in the nanocomposite with a higher initial particle loading. The saturation magnetization in the nanocomposite with high particle loading was larger, and the conduction behavior follows a three-dimensional variable range hopping mechanism. The presence of the iron oxide nanoparticles in the nanocomposites is observed to produce a more condensed structured PPy. The decreased conductivity in the high particle loading is due to the insulating behavior of iron oxide. Compared to mechanical stirring, ultrasonic stirring plays a critical role in the iron oxide-PPy nanocomposite formation and provides protection of iron oxide nanoparticles from dissolution by protons arising from a tight PPy matrix formed surrounding the iron oxide nanoparticles.

Acknowledgments The present paper is based on work supported by QuantumSphere Research Grant (QuantumSphere Inc.), UC-discovery Grant ELE06-10268, and the Air Force Office of Scientific Research Grant F9550-05-1-0138. DPY kindly acknowledges support from the National Science Foundation under Grant No. DMR 04-49022.

References

Abthagir PS, Saraswathi R (2005) Thermal stability of polypyrrole prepared from a ternary eutectic melt. Mater Chem Phys 92:21–26

Asavapiriyanont S, Chandler GK, Gunawardena GA, Pletcher D (1984) The electrodeposition of polypyrrole films from aqueous solutions. J Electroanal Chem 177:229–244

An KH, Jeong SY, Hwang HR, Lee YH (2004) Enhanced sensitivity of a gas sensor incorporating single-walled carbon nanotube-polypyrrole nanocomposites. Adv Mater 16:1005–1009

Beek W, Wienk MM, Jassen RAJ (2004) Efficient hybrid solar cells from zinc oxide nanoparticles and a conjugated polymer. Adv Mater 16:1009–1013

Bi S, Wei X, Li N, Lei Z (2008) In-situ formation of Fe_3O_4 nanoparticles within the thermosensitive hairy hybrid particles. Mater Lett 62:2963–2966

Brosseau C, Talbot P (2005) Effective magnetic permeability of Ni and Co Micro- and nanoparticles embedded in a ZnO matrix. J Appl Phys 97:104325

Castro C, Ramos J, Millan A, Gonzalez-Calbet J, Palacio F (2000) Production of magnetic nanoparticles in imine polymer matrixes. Chem Mater 12:3681–3688

Chen W, Li X, Xue G, Wang Z, Zou W (2003) Magnetic and conducting particles: preparation of polypyrrole layer on Fe_3O_4 nanospheres. Appl Surf Sci 218:215–221

Chen Y, Sun L, Chiparus O, Negulescu I, Yachmenev V, Warnock M (2005) Kenaf/Ramie Composite for automotive headliner. J Polym Environ 13:107–114

Corbierre MK, Cameron NS, Sutton M, Mochrie SGJ, Lurio LB, Ruehm A, Lennox RB (2001) Polymer-stabilized gold nanoparticles and their incorporation into polymer matrices. J Am Chem Soc 123:10411–10412

Dey A, De A, De SK (2005) Electrical transport and dielectric relaxation in Fe_3O_4-polypyrrole hybrid nanocomposites. J Phys Condens Matter 17:5895–5910

Dutta K, De SK (2006) Transport and optical properties of SiO_2-polypyrrole nanocomposites. Solid State Commun 140:167–171

Ferreira CA, Aeiyach S, Delamar M, Lacaze PC (1990) Electropolymerization of pyrrole on iron electrodes Influence of solvent and electrolyte on the nature of the deposits. J Electroanal Chem 284:351–369

Gall K, Dunn ML, Liu Y, Stefanic G, Balzar D (2004) Internal stress storage in shape memory polymer nanocomposites. Appl Phys Lett 85:290–292

Gangopadhyay R, De A, Das S (2000) Transport properties of polypyrrole-ferric oxide conducting nanocomposites. J Appl Phys 87:2363–2367

Guo Z, Henry L, Palshin V, Podlaha EJ (2006) Synthesis of poly(methyl methacrylate) stabilized colloidal zero-valence metallic nanoparticles. J Mater Chem 16:1772–1777

Guo Z, Park S, Hahn HT, Wei S, Wei S, Moldovan M, Karki AB, Karki AB, Young DP (2007a) Magnetic and electromagnetic evaluation of the magnetic nanoparticle filled polyurethane nanocomposites. J Appl Phys 101:09M511

Guo Z, Park S, Hahn HT, Wei S, Moldovan M, Karki AB, Young DP (2007b) Giant magnetoresistance behavior of an iron/carbonized polyurethane nanocomposite. Appl Phys Lett 90:053111

Guo Z, Park S, Wei S, Pereira T, Moldovan M, Karki AB, Young DP, Hahn HT (2007c) Flexible high-loading particle-reinforced polyurethane magnetic nanocomposite fabrication through particle-surface-initiated polymerization. Nanotechnology 18:335704

Han G, Yuan J, Shi G, Wei F (2005) Electrodeposition of polypyrrole/multiwalled carbon nanotube composite films. Thin Solid Films 474:64–69

Huang K, Wan M, Long Y, Chen Z, Wei Y (2005) Multifunctional polypyrrole nanofibers via a functional dopant-introduced process. Syn Met 155:495–500

Ingram MD, Staesche H, Ryder KS (2004) 'Ladder-doped' polypyrrole: a possible electrode material for inclusion in electrochemical supercapacitors? J Power Sources 129:107–112

Kwon JD, Kim PH, Keum JH, Kim JS (2004) Polypyrrole/titania hybrids: synthetic variation and test for the photovoltaic materials. Sol Energy Mater Sol Cells 83:311–321

Lakard B, Segut O, Lakard S, Herlem G, Gharbi T (2007) Potentiometric miniaturized pH sensors based on polypyrrole films. Sens Actuators B 122:101–108

Lee K, Cho S, Park SH, Heeger AJ, Lee CW, Lee SH (2006) Metallic transport in polyaniline. Nature 44:65–68

Lee S, Shin HJ, Yoon SM, Yi DK, Choi JY, Paik U (2008) Refractive index engineering of transparent ZrO_2–polydimethyldiloxane nanocomposites. J Mater Chem 18:1751–1755

Lei Z, Bi S (2007) Preparation of polymer nanocomposites of core-shell structure via surface-initiated atom transfer radical polymerizations. Mater Lett 61:3531–3534

Li X, Wan M, Wei Y, Shen J, Chen Z (2006) Electromagnetic functionalized and core-shell micro/nanostructured polypyrrole composites. J phys Chem B 110:14623–14626

Li Y, Wei GX, Sue HJ (2002) Morphology and toughening mechanisms in clay-modified styrene-tutadiene-styrene rubber-toughened polypropylene. J Mater Sci 37: 2447–2459

Mack JJ, Viculis LM, Ali A, Luoh R, Yang G, Hahn HT, Ko FK, Kaner RB (2005) Graphite nanoplatelet reinforcement of electrospun polyacrylonitrile nanofibers. Adv Mater 17:77–80

Mammeri F, Bourhis EL, Rozes L, Sanchez C (2005) Mechanical properties of hybrid organic-inorganic materials. J Mater Chem 15:3787–3811

Mei Y, Zhou ZJ, Luo HL (1987) Electrical resistivity of rf-sputtered iron oxide thin films. J Appl Phys 61:4388–4389

Mohr R, Kratz K, Weigel T, Lucka-Gabor M, Moneke M, Lendlein A (2006) Initiation of shape-memory effect by inductive heating of magnetic nanoparticles in thermoplastic polymers. Proc Natl Acad Sci 103:3540–3545

Noh KA, Kim DW, Jin CS, Shin KH, Kim JH, Ko JM (2003) Synthesis and pseudo-capacitance of chemically-prepared polypyrrole powder. J Power Sources 124:593–595

Omastova M, Boukerma K, Chehimi MM, Trchova M (2005) Novel silicon carbide/polypyrrole composite; preparation and physicochemical properties. Mat Res Bull 40: 749–765

Ortiz C, Lim G, Chen MM, Castillo G (1988) Physical properties of spinel iron oxide thin films. J Mater Res 3:344–350

Podlaha EJ, Li Y, Zhang J, Huang Q, Panda A, Lozano-Morales A, Davis D, Guo Z (2006) Nanomaterials Handbook Y Gogotsi (ed) Boca Raton, FL: CRC Press, 475

Ram S (1995) Infrared study of the dynamics of boroxol rings in the crystallization of $BaFe_{12}O_{19}$ microcrystals in borate glasses. Phys Rev B 51:6280–6286

Sepulveda-guzman S, Lara L, Perez-Camacho O, Rodriguez-Fernandez O, Olivas A, Escudero R (2007) Synthesis and characterization of an iron oxide poly(styrene-co-carboxybutylmaleimide) ferrimagnetic composite. Polymer 48:720–727

Song HK, Palmore GTR (2006) Redox-active polypyrrole: toward polymer-based batteries. Adv Mater 2006(18):1764–1768

Su SJ, Kuramoto N (2000) Processable polyaniline-titanium dioxide nanocomposites: effect of titanium dioxide on the conductivity. Syn Met 114:147–153

Suri K, Annapoorni S, Tandon RP (2001) Phase change induced by polypyrrole in iron-oxide polypyrrole nanocomposite. Bull Mater Sci 24:563–567

Suri K, Annapoorni A, Tandon RP, Rath C, Aggrawal VK (2003) Thermal transition behavior of iron oxide-polypyrrole nanocomposites. Curr Appl Phy 3:209–213

Tandon RP, Tripathy MR, Arora AK, Hotchandani S (2006) Gas and humidity response of iron oxide-polypyrrole nanocomposites. Sens Actuators B 114:768–773

Toal SJ, Trogler WC (2006) Polymer sensors for nitroaromatic explosives detection. J Mater Chem 2006(16):2871–2883

Vivekchand S, Kam KC, Gundiah G, Govindaraj A, Cheetham AK, Rao CNR (2005) Electric properties of inorganic nonowire-polymer composites. J Mater Chem 15:4922–4927

Wang L, Rocci-Lane M, Brazis P, Kannewurf CR, Kim YI, Lee W, Choy JH, Kanatzidis MG (2000) R-$RuCl_3$/polymer nanocomposites: the first group of intercalative nanocomposites with transition metal halides. J Am Chem Soc 122:6629–6640

Wetzel B, Haupert F, Zhang MQ (2003) Epoxy nanocomposites with high mechanical and tribological performance. Comp Sci Technol 63:2055–2067

Yeh JM, Chin CP, Chang S (2003) Enhanced corrosion protection coatings prepared from soluble electronically conductive polypyrrole-clay nanocomposite materials. J Appl Polym Sci 88:3264–3272

Yen SJ, Chen EC, Chiang RK, Wu TM (2008) Preparation and characterization of polypyrrole/magnetite nanocomposites synthesized by in situ chemical oxidative polymerization. J Polym Sci B; Polym Phys 46:1291–1300

Yuvaraj H, Woo MH, Park EJ, Jeong YT, Lim KT (2008) Polypyrrole/γ-Fe_2O_3 magnetic nanocomposites synthesized in supercritical fluid. Eur Polym J 44:637–644

Zaid B, Aeiyach S, Lacaze PC (1994) Electropolymerization of pyrrole in propylene carbonate on zinc electrodes modified by heteropolyanions. Syn Met 65:27–34